Erschienen in: Immunity ; 44 (2016), 1. - S. 59-72
https://dx.doi.org/10.1016/j.immuni.2015.12.010

Inflammation-Induced CCR7 Oligomers Form Scaffolds to Integrate Distinct Signaling Pathways for Efficient Cell Migration

Mark A. Hauser,[1] Karin Schaeuble,[1,5] Ilona Kindinger,[1] Daniela Impellizzieri,[2] Wolfgang A. Krueger,[3] Christof R. Hauck,[4] Onur Boyman,[2] and Daniel F. Legler[1,*]
[1]Biotechnology Institute Thurgau (BITg) at the University of Konstanz, 8280 Kreuzlingen, Switzerland
[2]Department of Immunology, University Hospital Zurich, University of Zurich, 8044 Zurich, Switzerland
[3]Klinikum Konstanz, 78464 Konstanz, Germany
[4]Chair of Cell Biology, University of Konstanz, 78464 Konstanz, Germany
[5]Present address: Department of Biochemistry, University of Lausanne, 1066 Epalinges, Switzerland
*Correspondence: daniel.legler@bitg.ch

SUMMARY

Host defense depends on orchestrated cell migration guided by chemokines that elicit selective but biased signaling pathways to control chemotaxis. Here, we showed that different inflammatory stimuli provoked oligomerization of the chemokine receptor CCR7, enabling human dendritic cells and T cell subpopulations to process guidance cues not only through classical G protein-dependent signaling but also by integrating an oligomer-dependent Src kinase signaling pathway. Efficient CCR7-driven migration depends on a hydrophobic oligomerization interface near the conserved NPXXY motif of G protein-coupled receptors as shown by mutagenesis screen and a CCR7-SNP demonstrating super-oligomer characteristics leading to enhanced Src activity and superior chemotaxis. Furthermore, Src phosphorylates oligomeric CCR7, thereby creating a docking site for SH2-domain-bearing signaling molecules. Finally, we identified CCL21-biased signaling that involved the phosphatase SHP2 to control efficient cell migration. Collectively, our data showed that CCR7 oligomers serve as molecular hubs regulating distinct signaling pathways.

INTRODUCTION

Acute inflammation is the host's major reaction to invading pathogens and the coordinated recruitment of cells to distinct sites is a hallmark of the immune system to eliminate the intruder (Medzhitov, 2010). Locally residing dendritic cells (DCs) sense the invading pathogen and transport antigens to the draining lymph nodes to launch a pathogen-specific adaptive immune response involving T and B cells (Joffre et al., 2009). Orchestrated migration of antigen-loaded DCs and T cells to secondary lymphoid organs relies on the chemokine receptor CCR7 and its two ligands, CCL19 and CCL21; alterations within the CCR7-CCL19/CCL21 axis severely impair both immunity and tolerance (Comerford et al., 2013; Förster et al., 2008). Of note, DCs encountering infectious or inflammatory insults undergo maturation and induce CCR7 expression. Lymphatic endothelial cells in the skin constitutively produce CCL21, forming a chemokine gradient (Weber et al., 2013). This haptotactic chemokine gradient guides CCR7-expressing DCs from the perilymphatic interstitium into the lymphatic capillaries. DCs are then transported by the lymph flow into the subcapsular sinus of the draining lymph node from where DCs again actively migrate along a CCL21 gradient established between the T zone and the subcapsular sinus (Ulvmar et al., 2014). Circulating CCR7-expressing T cells enter lymph nodes through high endothelial venules, where presented CCL21 facilitates integrin activation and entrance. Subsequently, CCR7 signaling contributes to intranodal motility of T cells and their encounter with antigen-bearing DCs (Braun et al., 2011).

Given the importance of CCR7 and its ligands in immunity and tolerance, tightly regulated production of both receptor and ligands have been reported to ensure appropriate responses (Comerford et al., 2013). In addition, several post-translational mechanisms have been observed to regulate cell responses to CCL19 and CCL21. Most prominently, inflammatory signals (MartIn-Fontecha et al., 2003) and the inflammatory lipid mediator prostaglandin (PG)E_2 (Kabashima et al., 2003; Legler et al., 2006) were identified as key factors for fast and efficient DC migration and homing to lymph nodes. Despite this key function, the underpinning molecular mechanism is unknown.

Chemokine receptors belong to the class A of G protein-coupled receptors (GPCRs) and utilize heterotrimeric G proteins to initiate signal transduction. Most chemokine-driven signaling events rely on pertussis toxin (PTx)-sensitive $G\alpha_i$ protein coupling, including those responsible for lymph node homing (Thelen and Stein, 2008). However, recent discoveries point to alternative but poorly defined signaling possibilities of chemokine receptors. Most conspicuously, effector T cells—in contrast to naive T cells—were shown to exploit Src kinase activity to bypass chemokine-mediated $G\alpha_i$ protein signaling to arrest and crawl on inflamed vessels (Shulman et al., 2012). The relatively new concept by which a GPCR ligand can preferentially activate one of several available signaling pathways is termed biased signaling (Rajagopal et al., 2010; Steen et al., 2014).

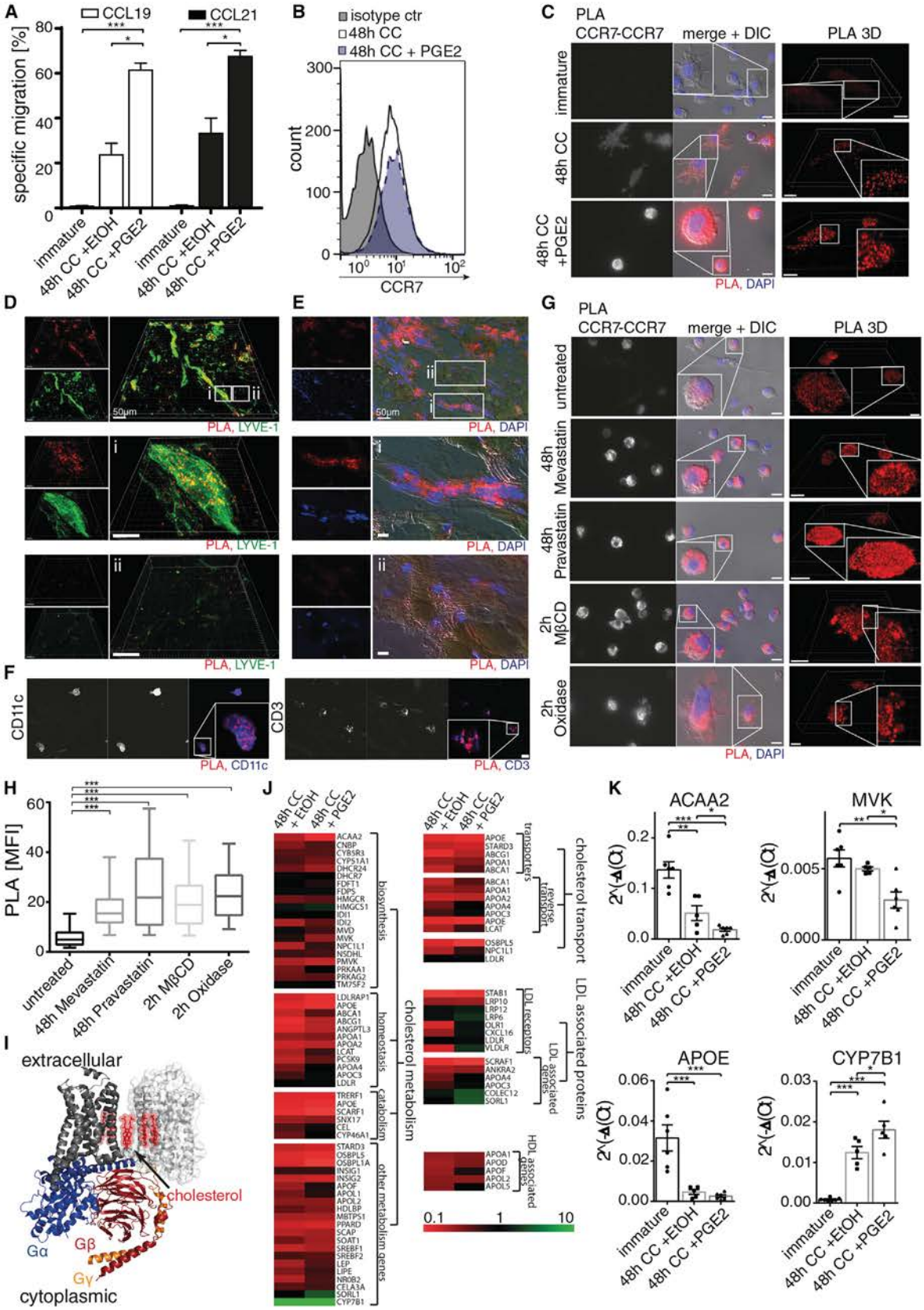

(legend on next page)

Notably, selective signaling by CCL19 and CCL21 have been identified downstream of CCR7. CCL21, through its unique, highly charged C-terminal extension, binds to glycosaminoglycans, becomes immobilized, and drives integrin-mediated adhesion and migration (Schumann et al., 2010). Conversely, only CCL19 induces robust CCR7 phosphorylation on Ser/Thr residues (Kohout et al., 2004) by G protein-coupled receptor kinase 3 (Zidar et al., 2009), resulting in β-arrestin recruitment and CCR7 internalization (Otero et al., 2006). How the two ligands can trigger distinct CCR7 signaling pathways remains poorly understood.

The complexity of chemokine signaling is further enlarged by receptor homo- and hetero-oligomerization. Both allosteric inhibition and synergistic activation of chemokine receptor hetero-oligomerization have been reported for various receptor pairs (Stephens and Handel, 2013). For CCR7, it is interesting to note that HIV-1 was shown to evoke CXCR4 signaling promoting CCR7-mediated $CD4^+$ T cell responses through an unknown mechanism that possibly involves oligomerization (Hayasaka et al., 2015). Recent structural discoveries derived from non-chemokine receptors revealed that in a GPCR dimer, only one receptor is able to interact with the G protein and that the G protein-free GPCR is capable to allosterically modulate the signaling outcome of the receptor dimer (Han et al., 2009; Huang et al., 2013). This might provide a new twist for understanding functional consequences of chemokine receptor oligomerization. Inspired by these findings, we posed the question as to whether environmental conditions, such as inflammatory stimuli, are able to modulate the oligomerization state of CCR7, enabling alternative signaling that accounts for efficient T cell and DC migration.

Here, we identified that an inflammatory signal mediated by PGE_2 provoked CCR7 oligomerization on human monocyte-derived (Mo)DCs, resulting in efficient migration. The same signals were found to downregulate the cholesterol metabolism in MoDCs. Cells treated with cholesterol-lowering drugs enhanced CCR7 oligomerization, so we proposed that PGE_2 lowers cholesterol levels to promote CCR7 oligomerization and efficient DC migration. Moreover, we identified CCR7 oligomers on DCs proximal to lymphatic vessels in human skin. In addition, we showed that CCR7 oligomers functioned to integrate G protein-dependent and Src kinase-dependent signaling at the GPCR oligomer. By using directed evolutionary screening, we developed the concept that efficient CCR7-driven cell migration depended on receptor oligomerization. This concept was substantiated by the identification of a CCR7-SNP owning super-oligomer characteristics manifested by enhanced Src activity and superior chemotaxis. Furthermore, we discovered that Src tyrosine phosphorylated CCR7 and demonstrated that this phosphorylation site served as docking site for SH2-domain-bearing signaling molecules. Finally, we identified a CCL21-biased signaling pathway involving the phosphatase SHP2 that controlled efficient cell migration.

RESULTS

PGE_2 Induces CCR7 Oligomerization and Promotes Efficient DC Migration

DCs reside as sentinels in the skin and mucosal tissue and sample the periphery for invading pathogens. After activation by infectious or inflammatory stimuli, DCs migrate into draining lymph nodes in a CCR7-dependent manner where they present peripherally acquired antigens to T cells, thereby launching an adaptive immune response. Notably, initiation of skin immune responses and DC homing is severely impaired in mice lacking the PGE_2 receptor EP4 (Kabashima et al., 2003). Similarly, human ex vivo DCs and MoDCs efficiently migrated in response to CCR7 ligands only if DCs were exposed to PGE_2 (Figure 1A; Legler et al., 2006). This pro-migratory DC phenotype could not be explained by PGE_2-mediated upregulation of CCR7 expression (Figure 1B) or by altered classical chemokine receptor signaling (Scandella et al., 2004). Because GPCR oligomerization is postulated to facilitate alternative signaling (Han et al., 2009), we thought to investigate whether PGE_2 triggering might modulate the oligomerization state of CCR7 and thereby facilitates efficient DC migration. To this end, we measured protein-protein interaction of endogenous CCR7 molecules in situ by proximity ligation assay (PLA). Indeed, profound CCR7 oligomerization, as manifested by red fluorescent dots, was most prominently found in human MoDCs matured in the presence of PGE_2 (Figure 1C). CCR7 oligomerization was also observed on activated, CD3/CD28-expanded human effector and central memory T cells (Figure S1A). CCR7 oligomers were also detected on freshly isolated PBLs and naive T cells but to a much lower amount (Figure S1A), suggesting that activation signals in general promoted

Figure 1. Inflammatory Signals Induce CCR7 Oligomerization and Cellular Cholesterol Depletion and Promote DC Migration

(A) Human MoDCs matured in the presence or absence of PGE_2 were subjected to 2D Transwell migration assays toward CCL19 and CCL21.

(B) Surface expression of CCR7 on human MoDCs matured in the presence (dashed black lines tinted blue) or absence (black line) of PGE_2 measured by flow cytometry. Isotype control in tinted light gray.

(C) Micrographs of DIC and confocal 3D reconstruction showing CCR7 oligomerization measured by PLA using anti CCR7 mAb (clone 6B3) on human MoDCs matured with cytokine cocktail (CC) in the presence or absence of PGE_2.

(D F) Micrographs of CCR7 oligomers determined by PLA using anti CCR7 mAb (clone 6B3) at LYVE 1^+ lymph vessels (D) or using anti CCR7 antibody (clone mab197) on $CD11c^+$ and $CD3^+$ cells (F) in snap frozen human skin sections (thickness: 8 μm). Squares indicate magnification for i (middle) and ii (bottom).

(G) Micrographs of DIC and confocal 3D reconstruction of CCR7 oligomers on human MoDCs matured with CC and PGE_2 in the absence (untreated) or presence of Mevastatin or Pravastatin. In addition, mature MoDCs were treated with MβCD or cholesterol oxidase for 2 hr.

(H) Quantification of CCR7 oligomerization upon cholesterol deprivation in MoDCs as shown in (G) from at least 190 cells from six individual experiments.

(I) Structural model of CCR7 and cholesterol (in red) at a putative CCR7 dimer interface based on solved crystal structures (PDB: 2RH1, 3SN6).

(J) Quantitative real time PCR analysis of genes in human MoDCs matured in the presence or absence of PGE_2. Fold change compared to 2^(−Δ(Ct)) values of immature MoDCs is depicted as a color coded heat map.

(K) Changes in the expression levels of selected genes depicted in (J) in MoDCs upon maturation and PGE_2 stimulation.

Data are from four to six independent experiments of individual donors (A H, J K). Error bars represent SD; ANOVA with Tukey (A, K) or Dunnett (H) post test. Scale bars represent 10 μm. See also Figure S1.

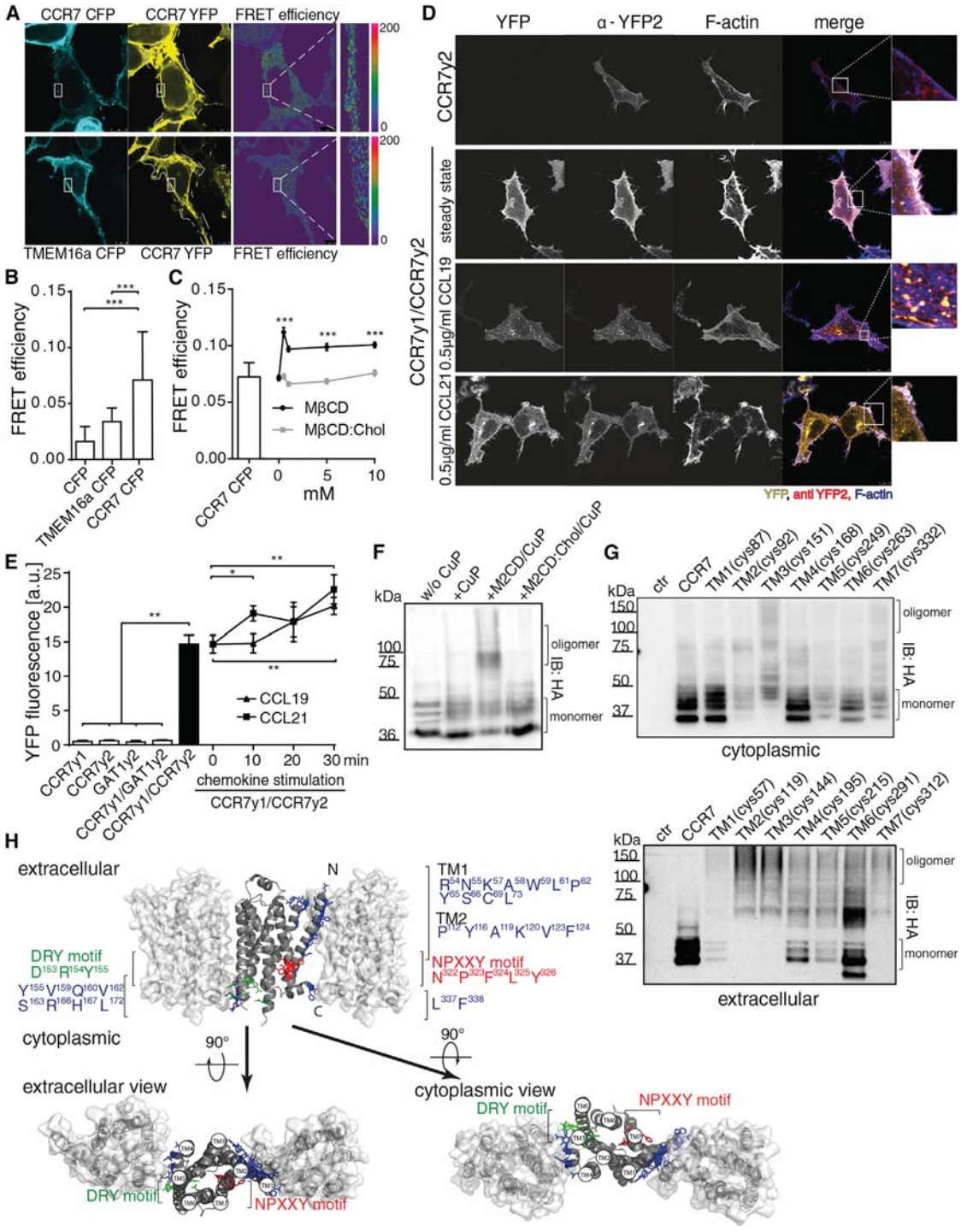

Figure 2. CCR7 Forms Oligomers in Steady State, Is Ligand and Cholesterol Sensitive, and Involves Two Interfaces

(A) Confocal image of CCR7 homo oligomerization and FRET efficiency determined by donor recovery after acceptor photo bleaching in HEK293 cell trans fectants.

(B and C) Quantification of FRET efficiency in HEK293 cells expressing CCR7 YFP and indicated constructs. Cells were treated or not with 5 mM MβCD or cholesterol pre saturated MβCD (C).

(D) Confocal image of CCR7 homo oligomerization determined by BiFC.

(E) Quantification of CCR7 oligomerization measured by BiFC and flow cytometry in HEK293 transfectants upon stimulation with 0.5 µg/ml chemokine.

(F) CCR7 oligomerization determined by chemical crosslinking of endogenous cysteines in non reducing SDS PAGE in HEK293 transfectants treated or not with MβCD or cholesterol pre saturated MβCD.

(G) CCR7 oligomerization deciphered by crosslinking cysteine residues introduced at indicated positions adjacent to the TM in non reducing SDS PAGE.

(legend continued on next page)

CCR7 oligomerization. In line with our observations on MoDCs, $CD45RO^+$ human T cells are reported to migrate more efficiently in response to CCL21 than $CD45RA^+$ T cells (Mayya et al., 2015). In our experimental setup, activated T cells migrate readily but less efficiently in response to CCR7 ligands (Schaeuble et al., 2011), but were more resistant to G protein inhibition by PTx (Figure S1B).

To explore CCR7 oligomerization in vivo, we measured CCR7-CCR7 interaction by PLA in human skin biopsies. CCR7 oligomerization was mainly found in proximity to LYVE-1-positive lymph vessels (Figures 1Di and 1Ei), but hardly in neighboring tissue distal from lymphatics (Figures 1Dii and 1Eii). Subsequent co-staining experiments revealed that cells possessing CCR7 oligomers were CD11c or CD3 positive (Figure 1F). Thus, we identified CCR7 oligomerization not only on cells that migrated into human skin lymphatics, but also on PGE_2-exposed MoDCs that readily migrated in response to CCR7 ligands, suggesting a role of CCR7 oligomerization in efficient cell migration.

PGE_2 Regulates Cellular Cholesterol Levels to Facilitate CCR7 Oligomerization on DCs

Because DC homing is impaired in inflammatory disease models where cholesterol accumulates in the skin (Angeli et al., 2004) and because cholesterol intercalation between two β2-AR molecules is shown to modulate the GPCR dimer interface (Figure 1I; Cherezov et al., 2007; Prasanna et al., 2014), we determined CCR7 oligomerization in MoDCs treated with low doses of cholesterol-lowering drugs (Mevastatin and Pravastatin to inhibit cholesterol biosynthesis; methyl-β-cyclodextrin [MβCD] to sequester plasma membrane cholesterol) and with cholesterol oxidase. Lowering cholesterol levels in MoDCs significantly increased CCR7 oligomerization (Figures 1G and 1H). Based on these observations, we examined whether DC maturation modulated the expression of enzymes for cholesterol biosynthesis. We found that MoDC maturation was accompanied by downregulation of major constituents of the cholesterol biosynthesis, metabolism, and transport pathways, whereas the cholesterol hydrolase CYP7B1 was significantly upregulated (Figures 1J and 1K). Notably, gene regulation of key enzymes controlling cellular cholesterol was significantly more pronounced in PGE_2-matured MoDCs (Figure 1K), indicating that PGE_2 enabled CCR7 oligomerization by lowering cellular cholesterol.

CCR7 Forms Homo-mers in Steady-State and Oligomerization Is Enhanced by Cholesterol Sequestration and Ligand Binding

Given our identification of CCR7 oligomerization on MoDCs and cells migrated into skin lymphatics, we were prompted to decipher the underlying mechanism. Therefore, we first conducted Förster resonance energy transfer (FRET) experiments by donor recovery after acceptor photo-bleaching between two CCR7 molecules. A marked FRET signal was measured between CCR7-CFP and CCR7-YFP in steady-state (Figures 2A, 2B, and S2A). The FRET signal was enhanced upon cholesterol sequestration (Figure 2C). Next, we used the split-YFP-based bimolecular fluorescence complementation (BiFC) approach (Nyfeler et al., 2005) to corroborate oligomerization, where two non-fluorescent YFP fragments were fused to two distinct CCR7 molecules. Upon CCR7 dimerization, the two non-fluorescent halves of YFP1 and YFP2 reconstituted to form a native YFP that emitted its fluorescent signal upon excitation (Figure S2B). Under steady-state conditions, CCR7 molecules were expressed as homo-dimers (Figure 2D). CCR7 dimerization was not due to molecular crowding and coincidental collision at the plasma membrane as shown by the fact that no hetero-dimerization was detected with increasing amounts of TMEM16a (Figure S2A) or by co-expressing the GABA transporter GAT1 (Figures 2E and S2C). CCR7 dimerization further increased upon CCL19 and CCL21 stimulation as assessed by BiFC and FRET (Figures 2E and S2D). Notably, complemented CCR7-YFP dimers were readily observed in endosomal vesicles upon CCL19 stimulation, demonstrating normal trafficking of the CCR7 oligomer (Figure 2D). Using chemical crosslinking of endogenous cysteines within CCR7 allowing us to distinguish a monomer from a crosslinked oligomer in non-reducing SDS-PAGE, we found that cholesterol sequestration by MβCD enhanced CCR7 dimerization as indicated by the high-molecular-weight band (Figure 2F). No molecular weight shift was observed upon treatment with cholesterol-saturated MβCD. Notably, cholesterol sequestration by MβCD not only facilitated CCR7 oligomerization but also enhanced CCR7-driven cell migration (Figure S2E). These findings demonstrated specific CCR7 oligomerization not only in the steady-state but also upon ligand stimulation and upon cholesterol sequestration.

Determining CCR7 Oligomerization Interfaces

To gain insight into the function of the CCR7 oligomer, we first aimed to identify the interfaces of the CCR7 oligomer by exploiting cysteine crosslinking. Therefore, we introduced individual cysteine residues at the beginning and end of every transmembrane domain (TM) of CCR7. The cysteine residues can be chemically crosslinked in case the TM domains are adjacent within a symmetric oligomer. We found that the introduced cysteines at the cytoplasmic end of TM3 and TM7 as well as the extracellular part of TM1, TM2, TM3, and TM7 could be crosslinked (Figure 2G). To develop testable hypotheses on the function of CCR7 oligomerization, we fitted the amino acid structures of CCR7 into solved crystal structures of oligomeric GPCRs by considering insights from the crosslinking experiment. As templates to model oligomeric CCR7, we used the oligomeric structures of β_2-AR (Figure 2H), CXCR4/μ-opioid-receptor (Figure S2F), and CCR5 (Figure S2G). All three CCR7 models predicted a first common oligomer interface comprising the end of TM7 and helix (HL)8. In contrast, the second oligomer interface differed substantially between models. Whereas the second

(H) Structure model of oligomeric CCR7 based on β_1 AR (PDB: 4GPO). Surfaces involved in the oligomer interfaces are in blue. Conserved GPCR domains are shown in green (DRY motif) and red (NPXXY motif). Side view, as well as views from the extracellular and the cytoplasmic surface of the oligomers, are shown.

Data represent three (D) or four independent experiments. Error bars represent SEM (B, C) or SD (E). ANOVA with Tukey post test. See also Figure S2.

oligomer interface of the β_2-AR- and the CCR5-based CCR7 model included the tip of TM1, TM2, and intracellular loop (ICL) 2 (Figures 2H and S2G), the second oligomer interface of the CXCR4-based CCR7 model included TM5 and TM6 (Figure S2F). To test the three CCR7 models, we generated CCR7 mutants where two key residues in either ICL2, HL8, or TM5 were replaced by alanines and expressed them in our split-YFP BiFC system. Because the alanine mutation in TM5 was expressed at the plasma membrane but did not influence CCR7 oligomerization (Figure S2H), we excluded the CXCR4-based CCR7 oligomerization model. In contrast, mutations in ICL2 and HL8 profoundly diminished CCR7 oligomerization but also prevented its surface expression (Figure S2H). The β_2-AR- and CCR5-based CCR7 models differed primarily in the symmetry of higher oligomers. In the β_2-AR-based CCR7 model, the oligomers were arranged as head-to-head and tail-to-tail tandems, whereas in the CCR5-based model, the oligomers were arranged in a stacked head-to-tail conformation. Because we could not further discriminate the two remaining models experimentally, we were considering both CCR7 oligomer models for further analysis. Nonetheless, we corroborated CCR7 oligomerization by identifying CCR7 oligomerization interfaces, one involving TM7 and HL8 and the other one comprising ICL2, TM1, and TM2, and we provided CCR7 oligomer models that could be tested functionally.

The Hydrophobic Interaction Surface Proximate to the NPXXY Motif in TM7 Is Key for CCR7 Oligomerization

To determine the functional consequence of CCR7 oligomerization, we next aimed to identify CCR7 mutants that were impaired in forming oligomers but remained readily expressed at the cell surface. To achieve this, we established and performed a directed evolutionary screen (Figure 3A) by which we cloned a library of CCR7 mutants randomly modified in ICL2 and TM7/HL8 into our split YFP1 vector. The library was then transfected into cells expressing wild-type CCR7-YFP2. Cells expressing CCR7 mutants that were no longer capable of reconstituting YFP due to the inability to form oligomers were sorted and the transfected plasmids were recovered, amplified, diversified by random mutagenesis, and re-transfected (Figure 3A). Then, we sorted cells that expressed CCR7 mutants at the plasma membrane but were negative for YFP complementation (Figure 3A). By sequencing the recovered plasmids, we identified distinct CCR7 mutants that all harbored single-point mutations in vicinity of the NPXXY motif of TM7 (Figures 3C and S3C). We performed plasmid titration transfection experiments and determined the oligomerization state of the CCR7 mutants using BiFC. The CCR7 mutants A315G (Figure 3B) and L325S (Figure S3A) showed profoundly reduced oligomerization compared to wild-type CCR7. Generating a CCR7 A315G,L325S double mutant further decreased the ability to oligomerize (Figure 3B). Notably, the identified oligomerization-defective mutants possessed a reduced hydrophobic interaction surface in the first oligomer interface of our oligomeric CCR7 models.

Generation and Identification of a Natural CCR7 Super-oligomerizer

Based on our finding that the hydrophobic interaction surface in the oligomer interface was key in determining the oligomerization state, we hypothesized that enlarging the hydrophobic surface near the NPXXY motif might further increase CCR7 oligomerization. Intriguingly, doubling the hydrophobic interaction surface by replacing A315 to valine created a CCR7 mutant behaving as super-oligomerizer (Figure 3B). Next, we wondered whether any natural SNP variant of CCR7 would follow this rule. By searching the public SNP database of NCBI (http://www.ncbi.nlm.nih.gov/projects/SNP), we indeed identified a natural G to A nucleotide polymorphism at position 1024 (SNP rs200720683), revealing a V317I substitution, occurring with a heterozygosity of 0.002, which exactly followed our rule. We cloned this CCR7 V317I SNP and demonstrated its super-oligomerization property by BiFC (Figure 3B). Taken together, we discovered that the hydrophobic surface of the oligomer interface build between TM7 and HL8 determined the oligomerization state of CCR7. Moreover, we identified CCR7 mutants that were impaired in forming oligomers and discovered a natural CCR7 SNP acting as super-oligomerizer.

Oligomerization State of CCR7 Determines Cell Migration Efficiency

Next, we generated immune cell lines expressing the CCR7 oligomer mutants to determine their migratory capacity. Significantly fewer cells expressing CCR7 mutants with reduced oligomerization state migrated in response to CCL19 and CCL21 in 2D Transwell assays (Figure 3D) and through 3D collagen I matrix (Figure S3B) as compared to cells expressing wild-type CCR7. In contrast, two to three times more cells expressing the super-oligomerizing CCR7 V317I SNP migrated toward CCL19 and CCL21 (Figures 3D and S3B). Hence, our data revealed that enhanced CCR7 oligomerization correlated with the capacity to promote efficient cell migration.

Next, we sought to design peptides mimicking the oligomer interfaces that ideally would intercalate between two CCR7 molecules, thereby interfering with receptor oligomerization. To strengthen the interaction of the peptides with the oligomer interface, we also designed peptides where amino acids were substituted to allow additional ionic interactions. Based on our CCR7 oligomerization models, we designed five different peptide candidates (Figures 3C and S3C). Incubation of cells expressing CCR7 split-YFP constructs with the peptides reduced CCR7 oligomerization (Figure S3D). Moreover, primary human T cells incubated with the intercalating peptides, but not with scrambled peptides, showed hampered cell migration in response to CCR7 ligands (Figure 3E) without downregulating CCR7 surface expression (Figure S3E).

Chemokine binding (Figure S3F) and G protein activation (Figures S3G and S3H) were similar for wild-type CCR7 and their oligomerization mutants, so it is tempting to speculate that CCR7 oligomerization promoted efficient cell migration through an additional signaling pathway aside from $G\alpha_i$ activation.

CCR7 Oligomer Serves as Signaling Scaffold for Src

Because effector T cell crawling on inflamed vessels relies on Src activity (Shulman et al., 2012) and because Src kinases modulate CCR7-driven T cell migration (Schaeuble et al., 2011), we investigated whether Src kinase interacted with the CCR7 oligomer. Src interacted with CCR7 in the steady state (Figures 4A and S4A). Src interaction with the CCR7 mutants with reduced oligomerization capacity (L325S, A315G,

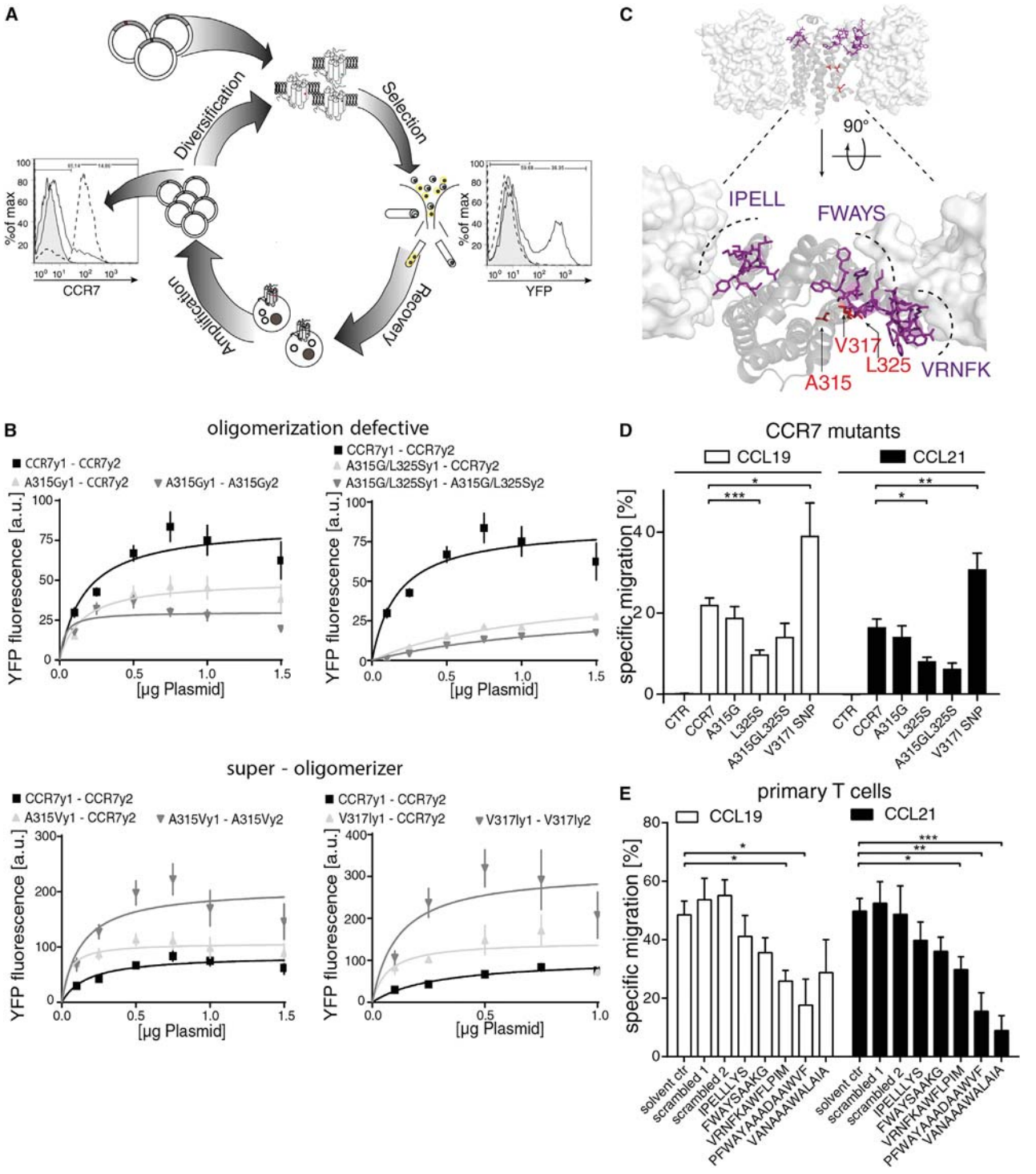

Figure 3. Cell Migration Efficiency Is Determined by the Oligomerization State of CCR7

(A) Illustration of the directed evolutionary screening to identify surface expressed, oligomer deficient CCR7 mutants.

(B) Determining the oligomerization state of CCR7 mutants and a natural CCR7 SNP measured by BiFC and quantified by flow cytometry in transiently transfected HEK293 cells.

(C) Localization of the mutants in the β_2 AR based CCR7 oligomer model. Residues involved in CCR7 oligomerization are in red. Designed peptides mimicking the oligomer interface for the inhibition study are shown in violet.

(D) Specific migration of 300 19 transfectants expressing CCR7 mutants in 2D Transwell chemotaxis assays toward 0.5 µg/ml CCL19 or CCL21.

(E) Specific Transwell migration of primary T cells treated with designed peptides mimicking the oligomer interface in response to chemokines.

Mean values ± SEM of four (E), six (D), or eight (B) experiments; ANOVA with Tukey post test. See also Figure S3.

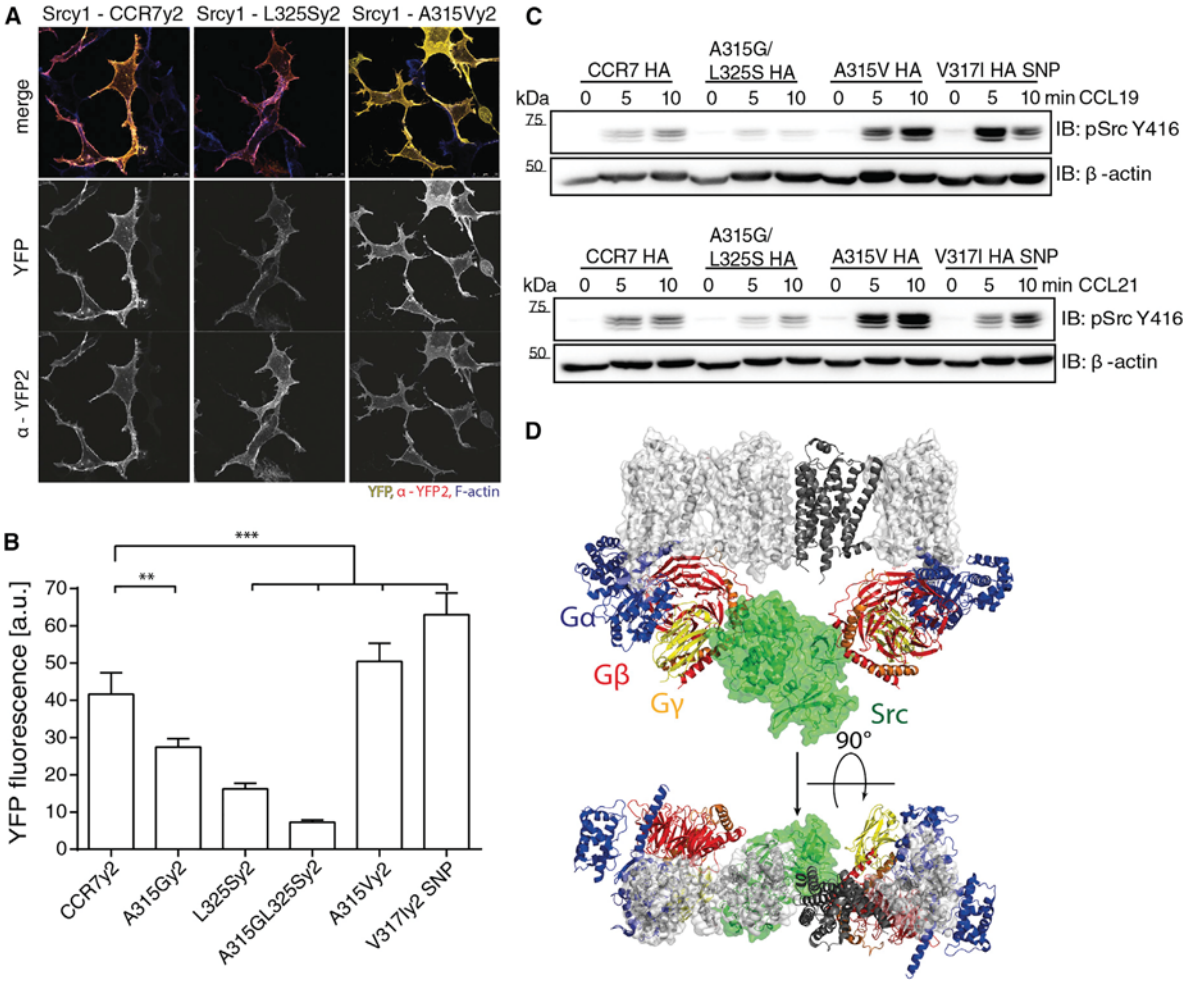

Figure 4. Src Associates with the CCR7 Oligomer and Becomes Activated upon Chemokine Stimulation

(A) Confocal image of the Src CCR7 interaction visualized by BiFC.

(B) Quantification of Src CCR7 interaction by BiFC and flow cytometry.

(C) Determining CCR7 mediated Src auto phosphorylation on Y416 in HEK293 cells expressing CCR7 variants by immunoblotting.

(D) Model of the CCR7 G protein Src complex.

Mean values ± SD of three (A, C) or six (B) experiments; ANOVA with Tukey post test. See also Figure S4.

A315G/L325S) was significantly reduced (Figures 4A and 4B). In contrast, both CCR7 super-oligomerizing mutants (A315V, V317I SNP) showed significantly augmented Src association (Figures 4A and 4B). CCR7 also interacted with Src in human MoDCs matured in the presence of PGE_2 (Figure S4B). Src had to be anchored to the plasma membrane to interact with CCR7 and required an intact SH3-SH2-linker motif, but not its kinase activity (Figures S4C–S4E). Moreover, CCR7 triggering induced auto-phosphorylation of Src on Y416 (Figure 4C). Notably, chemokine-mediated SrcY416 phosphorylation was strongly enhanced in cells expressing the CCR7 super-oligomerizers but severely impaired in cells expressing the oligomer-defective CCR7-A315G/L325S mutant (Figure 4C). CCR7-mediated SrcY416 phosphorylation was also confirmed in primary human PBLs (Figure S4F).

Structural insights from the β_2-AR-G protein complex on the one hand (Rasmussen et al., 2011) and the β_1-AR oligomer on the other hand (Huang et al., 2013) predict that in an oligomeric arrangement, a GPCR tetramer allows docking of only two G proteins, leaving two receptor molecules unoccupied (Huang et al., 2013). Hence, the question arose whether there could happen G protein-independent signaling by arranging two CCR7 dimers as tetramer with one associated trimeric G protein per dimer. Here, Src theoretically fitted into the free space between the G proteins (Figure 4D). In this CCR7 tetramer model, Src would interact not only with the two central receptors, but also with the G proteins bound to the outer receptors. To test this scenario, we monitored Src interaction with the G protein. Indeed, Src interacted not only with the CCR7-mer, but also with $G\alpha_i$, $G\beta_2$, and $G\gamma_2$ (Figures S4G and S4H), which is in line with the fact that Src is a direct effector of $G\alpha_i$ proteins in reconstituted systems (Ma et al., 2000). Astonishingly, at sites of Src-G protein interaction, numerous peripheral circular ruffles containing filamentous actin emerged (Figure S4G). Thus, our data

revealed that the interaction of CCR7 with Src depended on the oligomeric state of the receptor, establishing a new signaling scaffold to integrate G protein- and Src-dependent pathways.

Phosphorylation of CCR7 by Src Contributes to Efficient Cell Migration

We found that the interaction of Src with CCR7 depended on receptor oligomerization and that Src was auto-phosphorylated upon CCR7 triggering, so we examined whether Src was able to phosphorylate CCR7. Tyrosine phosphorylation (pTyr) of CCR7 was found exclusively upon chemokine stimulation (Figures 5A and S5A). Chemokine-induced CCR7 phosphorylation was completely abolished in cells pre-treated with the Src kinase inhibitor PP2, but not by blocking $G\alpha_i$ signaling via PTx (Figure 5B). In line with CCR7 oligomer-dependent Src interaction, chemokine-mediated pTyr of CCR7 was reduced in oligomerization-defective mutants, but enhanced in super-oligomerizers, including the CCR7 V317I SNP (Figure S5B). Moreover, robust chemokine-mediated pTyr of CCR7 was found in mature MoDCs, particularly in those cells exposed to PGE_2 (Figure 5C), corroborating oligomerization-dependent pTyr of CCR7. Because CCR2 has been shown to be phosphorylated on the conserved tyrosine of the DRY motif (Mellado et al., 1998), we mutated the corresponding Y155 of CCR7 to phenylalanine and found that chemokine-mediated pTyr was hampered (Figure 5D). Importantly, cells expressing CCR7 Y155F migrated profoundly less both in 2D and 3D toward CCL19 and CCL21 as compared to cells expressing wild-type CCR7 (Figures 5E and S5C). Because the DRY motif is essential for G protein coupling, we next examined whether the Y155F substitution affected G protein coupling. In contrast to a CCR7 R154N (DNY) mutant that was unable to activate $G\alpha_i$ and did not induce cell migration (Figures 5E, 5G, S5C, and S5D), we measured normal G protein activation and calcium mobilization upon chemokine binding in our CCR7 Y155F mutant (Figures 5G, S5D, and S5E). Of note, we demonstrated that not only G protein inhibition but also Src inhibition abrogated CCR7-mediated migration of primary human T cells (Figure 5F), although G protein inhibition was more effective. Taken together, we demonstrated not only that Src tyrosine phosphorylated CCR7, but also that Src inhibition and mutating the tyrosine residue within the DRY motif of CCR7 hampered cell migration.

Phosphorylated Y155 of CCR7 Serves as Docking Site for the Tyrosine Phosphatase SHP2

To further elucidate the new signaling pathway initiated by the CCR7 oligomer, we performed a screen to identify SH2 domains recognizing tyrosine-phosphorylated CCR7. Because SH2 domains are known interaction modules recognizing linear motifs including pTyr residues, we used a panel of purified GST-SH2-domain fusion proteins for screening (Figures S5F and S5G). The C-terminal SH2 domain of the tyrosine phosphatase SHP2 most effectively interacted with phosphorylated CCR7 (Figure S5H). SHP2 harbors two SH2 domains (Figure S5I). In its inactive conformation, the N-terminal SH2 domain is folded over the catalytic cleft, preventing interaction with its substrates (Neel et al., 2003). With its C-terminal SH2 domain, SHP2 surveys the cell for potential interaction partners. Upon binding of the C-terminal SH2 domain, auto-inhibition is relieved and SHP2 becomes catalytically active. To become fully activated, SHP2 needs to be phosphorylated on two tyrosine residues in its C terminus, resulting in interaction with phosphorylated residues and SH2 domains in *cis*. Using co-immunoprecipitation experiments, we confirmed that SHP2 was specifically recruited to CCR7 upon chemokine stimulation (Figure 6A). Of note, SHP2 was not recruited to the CCR7 Y155F mutant (Figure S6A). Because CCR7 phosphorylation was dependent on Src, we asked whether the interaction of CCR7 with SHP2 occurred in a G protein-parallel manner. To address this, we exploited a rapamycin-inducible active Src to determine SHP2 recruitment to CCR7 by BiFC. This approach allowed us to circumvent chemokine stimulation and G protein activation. We found that active Src was necessary and sufficient to recruit SHP2 to CCR7. No CCR7-SHP2 interaction was measurable in cells expressing either a kinase-dead mutant of Src or phosphorylation-deficient CCR7 Y155F (Figures 6B and S6B). Thus, we showed not only that pTyr residue of the DRY motif served as docking site for SH2-domain-containing proteins, such as SHP2, but also that Src was necessary and sufficient to induce this interaction.

Moreover, both CCL19 and CCL21 led to a rapid phosphorylation of SHP2 (Figure 6C) but not of SHP1 (Figure S6C) in primary human PBLs. Chemokine-mediated SHP2 phosphorylation was dependent on Src as shown by PP2 treatment of PBLs (Figure S6D). Chemokine-mediated SHP2 phosphorylation was independent of G protein coupling and could not be blocked by a JAK inhibitor (Figure S6D). The latter is interesting because JAK2 is shown to tyrosine phosphorylate CCR2 in a G protein-parallel but dimerization-dependent manner (Mellado et al., 1998).

Because SHP2 activity is highly regulated not only through binding to interaction partners or substrates but also through relief of auto-inhibition and interaction in *cis*, we aimed to examine the SHP2 activity after CCR7 stimulation. Therefore, we developed a phosphatase activity assay with a phospho-peptide as substrate (Figure S6E). In line with SHP2 phosphorylation, SHP2 catalytic activity co-immunoprecipitated with CCR7 was similarly triggered by both CCL19 and CCL21 (Figure S6E). Despite comparable SHP2 phosphorylation and catalytic activity at the receptor, CCL21 triggering resulted in several-fold higher cytosolic activity of SHP2 in T cells than CCL19 (Figure 6D). Thus, we provide the first evidence for a CCL21-induced biased signaling pathway through an additional cytosolic pool of SHP2 catalytic activity.

SHP2 Is Critical for Biased Signaling and Migration by CCL21

Knowing that SHP2 was activated upon CCR7 stimulation and that SHP2 was not involved in CCR7 de-phosphorylation (instead, SHP2 inhibition decreased CCR7 phosphorylation) (Figure 5D), we examined the role of SHP2 in CCR7-driven cell migration. Therefore, primary human T cells were pre-treated with the SHP inhibitor NSC-87877 or the SHP2 inhibitor PHPS1 to block SHP2 catalytic activity but not its adaptor function. Inhibition of SHP2 did not significantly affect CCL19-mediated T cell migration, whereas T cell migration toward CCL21 was severely impaired in cells treated with NSC-87877 (Figure 6E) or PHPS1 (Figure 6F). That SHP2 was critical for biased

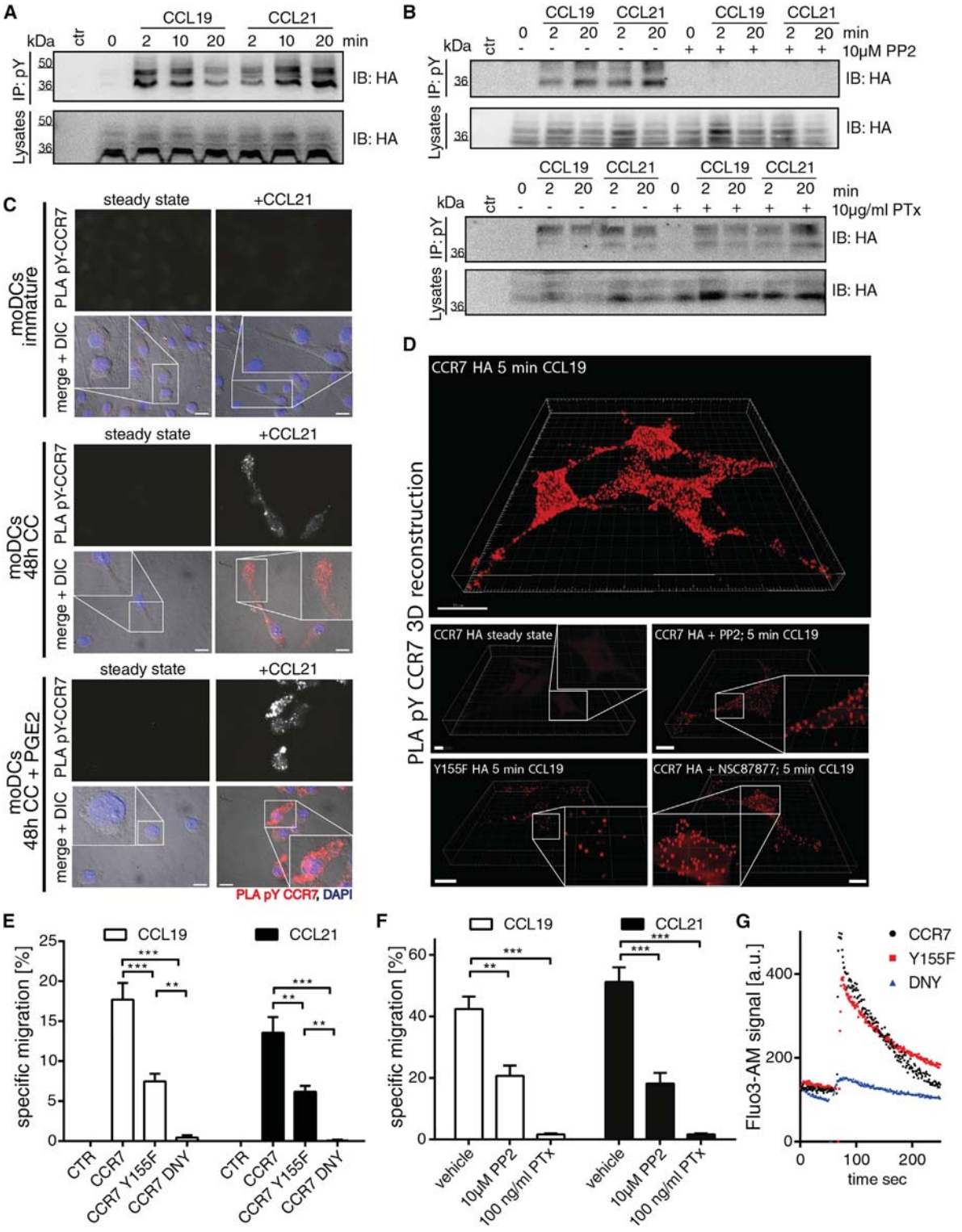

Figure 5. Src Tyrosine Phosphorylates CCR7 upon Chemokine Stimulation to Control Migration

(A) HA tagged CCR7 from CCL19 and CCL21 stimulated cells was immunoprecipitated (IP) from cell lysates and its tyrosine phosphorylation (pY) determined by immunoblotting.

(B) Determining CCR7 pTyr in cells treated with the Src inhibitor PP2 or the G protein coupling inhibitor PTx as in (A).

(C) Micrograph of CCR7 pTyr assessed by PLA using anti CCR7 Ab (SAB4500329) and anti pTyr mAb (4G10) in (CC ± PGE_2) matured MoDCs.

(legend continued on next page)

CCL21-driven migration was confirmed in human B cells and MoDCs (Figures 6G and 6H).

In summary, we established that CCR7 oligomerization generated a novel platform to integrate G protein- and Src-dependent signaling resulting in tyrosine phosphorylation of CCR7. Moreover, we demonstrated that this CCR7 phosphorylation served as docking site for SH2-domain-containing signaling proteins. Finally, we showed CCL21 biased signaling for efficient cell migration involving a cytosolic pool of catalytically active SHP2.

DISCUSSION

Here we described a previously unknown mechanism of how environmental cues control immune cell migration by modulating the oligomerization state of the chemokine receptor CCR7 enabling integration of distinct signaling pathways at the receptor oligomer interface. We identified that inflammatory signals and PGE_2 provoked oligomerization of CCR7 on DCs. The same signals led to a profound downregulation of genes involved in cholesterol biosynthesis and metabolism. Lowering cellular cholesterol levels by drugs interfered with CCR7 oligomerization and cell migration, so we propose that this represents a molecular mechanism by which only PGE_2-exposed DCs efficiently emigrate from inflammatory sites to home to draining lymph nodes (Kabashima et al., 2003; Legler et al., 2006). We showed that CCR7 oligomerization established a platform to elicit distinct signaling pathways controlling cell migration. Based on our oligomeric CCR7 model and experimental evidence, we proposed that within a tetrameric organization, two receptors couple to $G\alpha_i$ proteins to elicit the well-established "classical" chemokine receptor signaling pathway. In addition, this arrangement permitted Src kinase to interact with the uncoupled two CCR7 molecules of the tetrameric complex. Indeed, we found that Src interaction with CCR7 depended on the oligomerization state of the receptor and initiated a G protein parallel signaling pathway contributing to efficient cell migration.

The signaling hub function of oligomeric receptors is appealing because previous studies derived from other GPCRs proposed allosteric modulation of signaling by receptor dimerization (Han et al., 2009; Huang et al., 2013). The concept of eliciting two orthogonal and mechanistically separated signaling pathways is particularly practical at sites of infection because many bacteria produce toxins to target either regulatory GTPases or heterotrimeric G proteins of the host to circumvent the host defense (Aktories, 2011). One of these toxins, PTx, ADP ribosylates $G\alpha_i$ proteins to prevent chemokine-mediated receptor activation and leukocyte recruitment. Hence, CCR7 oligomerization and thereby establishing a signaling hub that allows simultaneous G protein-dependent and Src-dependent signaling pathways allows DCs to integrate distinct signaling pathways to ensure fast and efficient homing to draining lymph nodes. Interestingly, effector T cells also expressed CCR7 oligomers and their migration was less sensitive to PTx, permitting adaptation of signaling to environmental cues. This notion is in line with a previous study describing that antigen-experienced effector T cells evolved to bypass $G\alpha_i$ signaling on inflamed vessels in order to access the injured tissue (Shulman et al., 2012).

Despite their fundamental role in health and disease, pharmaceutical targeting of chemokine receptors has been difficult and of disappointing success. The low success has been attributed to the redundancy of chemokines acting on the same receptor. The discovery of biased signaling might be a solution for new attempts in developing new drugs. CCR7 represents a prototype receptor for biased signaling (Zidar et al., 2009). Whereas equal receptor-binding affinities and equal G protein activation (Kohout et al., 2004) suggests high redundancy in CCR7 signaling, some signaling characteristics appear to be unique to either CCL19 or CCL21. Most prominently, only CCL19 (and not CCL21) promotes CCR7 internalization (Otero et al., 2006). This CCL19 bias is reported to rely on robust phosphorylation on Ser/Thr residues in the C terminus of CCR7 by GRK3 and GRK6, resulting in stronger β-arrestin recruitment and ERK activation (Kohout et al., 2004; Zidar et al., 2009) and subsequent CCR7 internalization via clathrin-coated pits (Otero et al., 2006). CCL19-mediated CCR7 sequestration from the plasma membrane and its trafficking into clathrin-coated vesicles might limit its accessibility for downstream signaling molecules. Therefore, it came of no surprise that CCL19-triggered CCR7 phosphorylation is terminated on a short-term scale, whereas CCL21-mediated phosphorylation seemed to be more prolonged. Up to now, bias-signaling molecules have been described only for CCL19, not for CCL21. Herein, we showed that both CCL19 and CCL21 led to the recruitment and the release of the auto-inhibition of the tyrosine phosphatase SHP2, whereas only CCL21 triggering established a prominent pool of cytosolic active SHP2. Surprisingly, the phosphorylation status of SHP2 was found to be equal in cells stimulated with either CCL19 or CCL21. Because CCL19-triggered CCR7 is internalized and traffics via early endosomes to the trans-Golgi-network (Schaeuble et al., 2012), whereas CCL21-triggered CCR7 remains at the plasma membrane, we proposed that SHP2 catalytic activity was spatially controlled through the interaction of a second adaptor molecule in a spatio-temporal manner. Because CCL21-mediated CCR7 stimulation resulted in a prominent pool of catalytic active SHP2, it is not surprising to note that inhibition of SHP2 specifically hampered CCL21-driven, but not CCL19-driven, DC and lymphocyte migration.

Overall, our finding that the oligomerization state of CCR7 shapes cell migration together with the possibility to modulate CCR7 oligomerization by changing cholesterol levels, by using oligomer-intercalating peptides or by specifically inhibiting CCL21, but not CCL19-mediated migration, sets the

(D) Micrograph of a 3D reconstruction showing CCL19 mediated CCR7 pTyr by PLA in HEK293 cells expressing HA tagged wild type or Y155F CCR7 pretreated or not with 10 μM PP2 and 40 μM NSC87877.

(E) Specific Transwell cell migration toward CCL19 and CCL21 of 300 19 cells expressing a phosphorylation defective (CCR7 Y155F) and a G protein coupling deficient mutant (CCR7 DNY).

(F) Specific CCR7 dependent Transwell migration of primary human T cell migration pre treated for 2 hr with 10 μM PP2 or 100 ng/ml PTx.

(G) CCL19 mediated calcium mobilization in 300 19 transfectants expressing CCR7 mutants.

Data represent at least three experiments (A D, G). Mean ± SEM of six (E) or four (F) experiments; ANOVA with Tukey post test. See also Figure S5.

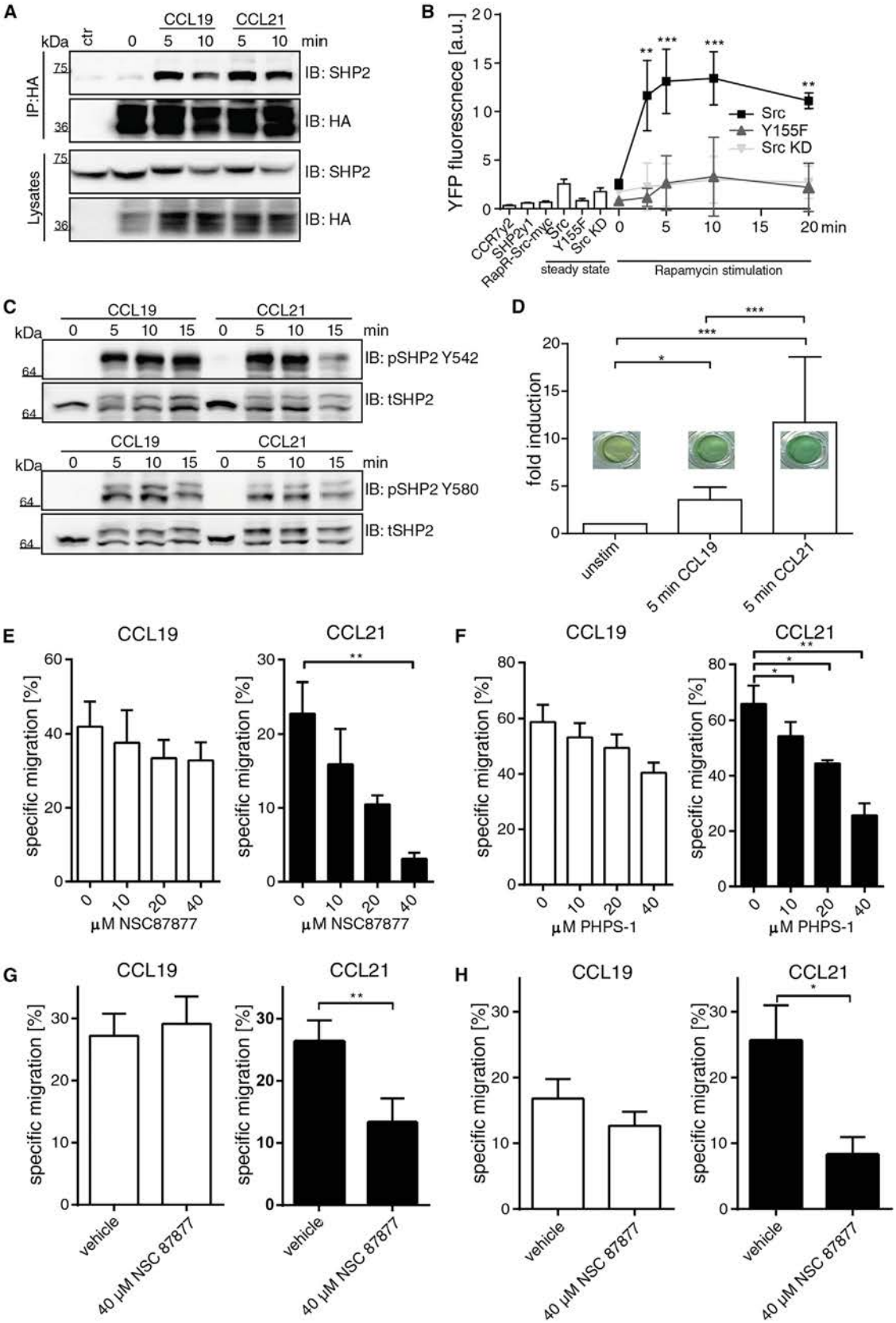

(legend on next page)

groundwork for biomedical implications. New ways of reducing CCR7-driven migration is desirable in the case of chronic inflammatory diseases or to prevent metastasis formation, whereas enhancing CCR7-driven migration would be highly appreciated in attempts to boost the immune system in a vaccine response.

EXPERIMENTAL PROCEDURES

Migration Assays

Cell migration in 2D was assessed with the Transwell systems with polycarbonate filters (Corning Costar). 3D migration was performed in bovine Purecol collagenI (3 mg/ml; Advanced Biomatrix). More details are provided in the Supplemental Experimental Procedures.

Proximity Ligation Assay

CCR7 CCR7 interaction was examined with reagents from the Duolink PLA (Sigma Aldrich). In brief, for cholesterol depletion, cells were pre incubated for 48 hr with 10 μM Mevastatin or 10 μM Pravastatin and for 2 hr with 0.6 M MβCD or 25 U/ml cholesterol oxidase. For visualization of pTyr CCR7, cells attached to cover slides were stimulated with 0.5 μg/ml CCL19/CCL21. Cells or snap frozen skin sections were fixed, blocked, and stained with primary antibody and secondary antibodies harboring short nucleotide sequences. Oligonucleotides were ligated at 37°C, and rolling circle PCR with fluorescent nucleotides was performed for 2 hr. PLA was visualized with an inverted confocal microscope. For further details see Supplemental Experimental Procedures.

Quantitative Real-Time PCR

Total RNA of MoDCs was isolated and transcribed into cDNA. Amplification of transcripts was performed with the Lipoprotein Signaling and Cholesterol Metabolism RT2 Profiler PCR Array (QIAGEN) on a 7900HT Fast Real Time PCR System (Applied Biosystems).

FRET Measurements

Intermolecular FRET efficiency was measured in HEK293 cells stably expressing CCR7 EYFP transiently transfected with either TMEM16a ECFP or CCR7 ECFP and fixed. A pre bleaching image was taken, and then the acceptor of the whole cell was bleached at 100% laser intensity and FRET efficiency was calculated. Further details are provided in the Supplemental Experimental Procedures.

BiFC Assay

HEK293 were co transfected with splitYFP1 and splitYFP2 tagged constructs and stimulated with 0.5 μg/ml CCL19 or CCL21. Fixed cells were detached and analyzed by flow cytometry. For immunofluorescence microscopy, cells were permeabilized and stained. Images were acquired by confocal microscopy. For further details see Supplemental Experimental Procedures.

Cys-Mediated Cross-linking

HEK293 cells transfected with HA tagged CCR7 were either pre treated with MβCD or not and reacted for 10 min at RT with 400 μM copper sulfate and 1,10 phenanthroline. Proteins were separated by SDS PAGE and detected by immunoblotting using an anti HA peroxidase antibody. Detailed information provided in Supplemental Experimental Procedures.

Co-immunoprecipitation

HEK293 expressing CCR7 HA or mutants thereof were starved, stimulated with chemokine, and subsequently incubated with 2.5 mM dithio bis succinimidyl propionate. Cells were lysed and HA tagged CCR7 was immunoprecipitated with anti HA agarose. Immunoprecipitated proteins were analyzed by immunoblotting. Detailed information provided in the Supplemental Experimental Procedures.

Statistical Evaluation

Significant differences between groups were assessed with ANOVA with either Tukey or Dunnett post test using GraphPad Prism v.6. *$p < 0.05$, ** $p < 0.01$, ***$p < 0.001$.

SUPPLEMENTAL INFORMATION

Supplemental Information includes six figures and Supplemental Experimental Procedures and can be found with this article online at http://dx.doi.org/10.1016/j.immuni.2015.12.010.

AUTHOR CONTRIBUTIONS

M.A.H. and D.F.L. designed the studies and wrote the manuscript. M.A.H., K.S., and I.K. performed all experiments and analyzed the data. D.I. and O.B. provided human skin biopsies. C.R.H. provided SH2 GST proteins. W.A.K. was responsible for collecting blood. D.F.L. supervised the overall study.

ACKNOWLEDGMENTS

We gratefully acknowledge Hesso Farhan for numerous advice and critical reading of the manuscript and Michael Sixt and Marcus Groettrup for support. This study was supported by grants from the Swiss National Science Foundation (SNF 31003A 143841), the Novartis Foundation for medical biological research, the Thurgauische Stiftung für Wissenschaft und Forschung, the Swiss State Secretariat for Education, Research and Innovation, and the Thurgauische Krebsliga to D.F.L.

Received: June 1, 2015
Revised: September 14, 2015
Accepted: October 16, 2015
Published: January 19, 2016

REFERENCES

Aktories, K. (2011). Bacterial protein toxins that modify host regulatory GTPases. Nat. Rev. Microbiol. *9*, 487 498.

Angeli, V., Llodrá, J., Rong, J.X., Satoh, K., Ishii, S., Shimizu, T., Fisher, E.A., and Randolph, G.J. (2004). Dyslipidemia associated with atherosclerotic disease systemically alters dendritic cell mobilization. Immunity *21*, 561 574.

Braun, A., Worbs, T., Moschovakis, G.L., Halle, S., Hoffmann, K., Bölter, J., Münk, A., and Förster, R. (2011). Afferent lymph derived T cells and DCs use different chemokine receptor CCR7 dependent routes for entry into the lymph node and intranodal migration. Nat. Immunol. *12*, 879 887.

Cherezov, V., Rosenbaum, D.M., Hanson, M.A., Rasmussen, S.G., Thian, F.S., Kobilka, T.S., Choi, H.J., Kuhn, P., Weis, W.I., Kobilka, B.K., and Stevens, R.C.

Figure 6. SHP2 Is Recruited to Tyrosine Phosphorylated CCR7 and Contributes to Biased CCL21 Driven Cell Migration

(A) Co immunoprecipitation (IP) of SHP2 with HA tagged CCR7 from stably transfected HEK293 cells upon stimulation with 0.5 μg/ml chemokine.

(B) SHP2 recruitment to CCR7 by a rapamycin inducible active or kinase dead Src in the absence of chemokines determined by BiFC in cells expressing SHP2 YFP1 and YFP2 tagged CCR7 or CCR7 Y155F.

(C) Chemokine triggered SHP2 phosphorylation on Y542 and Y580 in primary human PBLs as assessed by immunoblotting.

(D) Analysis of the SHP2 phosphatase activity in SHP2 immunoprecipitates of PBLs triggered by chemokines as described in the Supplemental Experimental Procedures.

(E H) Specific Transwell migration of primary human T cells (E, F), $CD19^+$ blood B cells (G), or mature MoDCs pre treated with NSC87877 (E, G, H) or the SHP2 specific inhibitor PHPS 1 (F).

Data represent four experiments. Error bars represent SD; ANOVA with Tukey post test. See also Figure S6.

(2007). High resolution crystal structure of an engineered human beta2 adrenergic G protein coupled receptor. Science *318*, 1258 1265.

Comerford, I., Harata Lee, Y., Bunting, M.D., Gregor, C., Kara, E.E., and McColl, S.R. (2013). A myriad of functions and complex regulation of the CCR7/CCL19/CCL21 chemokine axis in the adaptive immune system. Cytokine Growth Factor Rev. *24*, 269 283.

Förster, R., Davalos Misslitz, A.C., and Rot, A. (2008). CCR7 and its ligands: balancing immunity and tolerance. Nat. Rev. Immunol. *8*, 362 371.

Han, Y., Moreira, I.S., Urizar, E., Weinstein, H., and Javitch, J.A. (2009). Allosteric communication between protomers of dopamine class A GPCR dimers modulates activation. Nat. Chem. Biol. *5*, 688 695.

Hayasaka, H., Kobayashi, D., Yoshimura, H., Nakayama, E.E., Shioda, T., and Miyasaka, M. (2015). The HIV 1 Gp120/CXCR4 axis promotes CCR7 ligand dependent CD4 T cell migration: CCR7 homo and CCR7/CXCR4 hetero oligomer formation as a possible mechanism for up regulation of functional CCR7. PLoS ONE *10*, e0117454.

Huang, J., Chen, S., Zhang, J.J., and Huang, X.Y. (2013). Crystal structure of oligomeric β1 adrenergic G protein coupled receptors in ligand free basal state. Nat. Struct. Mol. Biol. *20*, 419 425.

Joffre, O., Nolte, M.A., Spörri, R., and Reis e Sousa, C. (2009). Inflammatory signals in dendritic cell activation and the induction of adaptive immunity. Immunol. Rev. *227*, 234 247.

Kabashima, K., Sakata, D., Nagamachi, M., Miyachi, Y., Inaba, K., and Narumiya, S. (2003). Prostaglandin E2 EP4 signaling initiates skin immune responses by promoting migration and maturation of Langerhans cells. Nat. Med. *9*, 744 749.

Kohout, T.A., Nicholas, S.L., Perry, S.J., Reinhart, G., Junger, S., and Struthers, R.S. (2004). Differential desensitization, receptor phosphorylation, beta arrestin recruitment, and ERK1/2 activation by the two endogenous ligands for the CC chemokine receptor 7. J. Biol. Chem. *279*, 23214 23222.

Legler, D.F., Krause, P., Scandella, E., Singer, E., and Groettrup, M. (2006). Prostaglandin E2 is generally required for human dendritic cell migration and exerts its effect via EP2 and EP4 receptors. J. Immunol. *176*, 966 973.

Ma, Y.C., Huang, J., Ali, S., Lowry, W., and Huang, X.Y. (2000). Src tyrosine kinase is a novel direct effector of G proteins. Cell *102*, 635 646.

MartIn Fontecha, A., Sebastiani, S., Höpken, U.E., Uguccioni, M., Lipp, M., Lanzavecchia, A., and Sallusto, F. (2003). Regulation of dendritic cell migration to the draining lymph node: impact on T lymphocyte traffic and priming. J. Exp. Med. *198*, 615 621.

Mayya, V., Neiswanger, W., Medina, R., Wiggins, C.H., and Dustin, M.L. (2015). Integrative analysis of T cell motility from multi channel microscopy data using TIAM. J. Immunol. Methods *416*, 84 93.

Medzhitov, R. (2010). Inflammation 2010: new adventures of an old flame. Cell *140*, 771 776.

Mellado, M., Rodríguez Frade, J.M., Aragay, A., del Real, G., Martín, A.M., Vila Coro, A.J., Serrano, A., Mayor, F., Jr., and Martínez A, C. (1998). The chemokine monocyte chemotactic protein 1 triggers Janus kinase 2 activation and tyrosine phosphorylation of the CCR2B receptor. J. Immunol. *161*, 805 813.

Neel, B.G., Gu, H., and Pao, L. (2003). The 'Shp'ing news: SH2 domain containing tyrosine phosphatases in cell signaling. Trends Biochem. Sci. *28*, 284 293.

Nyfeler, B., Michnick, S.W., and Hauri, H.P. (2005). Capturing protein interactions in the secretory pathway of living cells. Proc. Natl. Acad. Sci. USA *102*, 6350 6355.

Otero, C., Groettrup, M., and Legler, D.F. (2006). Opposite fate of endocytosed CCR7 and its ligands: recycling versus degradation. J. Immunol. *177*, 2314 2323.

Prasanna, X., Chattopadhyay, A., and Sengupta, D. (2014). Cholesterol modulates the dimer interface of the β_2 adrenergic receptor via cholesterol occupancy sites. Biophys. J. *106*, 1290 1300.

Rajagopal, S., Rajagopal, K., and Lefkowitz, R.J. (2010). Teaching old receptors new tricks: biasing seven transmembrane receptors. Nat. Rev. Drug Discov. *9*, 373 386.

Rasmussen, S.G., DeVree, B.T., Zou, Y., Kruse, A.C., Chung, K.Y., Kobilka, T.S., Thian, F.S., Chae, P.S., Pardon, E., Calinski, D., et al. (2011). Crystal structure of the β2 adrenergic receptor Gs protein complex. Nature *477*, 549 555.

Scandella, E., Men, Y., Legler, D.F., Gillessen, S., Prikler, L., Ludewig, B., and Groettrup, M. (2004). CCL19/CCL21 triggered signal transduction and migration of dendritic cells requires prostaglandin E2. Blood *103*, 1595 1601.

Schaeuble, K., Hauser, M.A., Singer, E., Groettrup, M., and Legler, D.F. (2011). Cross talk between TCR and CCR7 signaling sets a temporal threshold for enhanced T lymphocyte migration. J. Immunol. *187*, 5645 5652.

Schaeuble, K., Hauser, M.A., Rippl, A.V., Bruderer, R., Otero, C., Groettrup, M., and Legler, D.F. (2012). Ubiquitylation of the chemokine receptor CCR7 enables efficient receptor recycling and cell migration. J. Cell Sci. *125*, 4463 4474.

Schumann, K., Lämmermann, T., Bruckner, M., Legler, D.F., Polleux, J., Spatz, J.P., Schuler, G., Förster, R., Lutz, M.B., Sorokin, L., and Sixt, M. (2010). Immobilized chemokine fields and soluble chemokine gradients cooperatively shape migration patterns of dendritic cells. Immunity *32*, 703 713.

Shulman, Z., Cohen, S.J., Roediger, B., Kalchenko, V., Jain, R., Grabovsky, V., Klein, E., Shinder, V., Stoler Barak, L., Feigelson, S.W., et al. (2012). Transendothelial migration of lymphocytes mediated by intraendothelial vesicle stores rather than by extracellular chemokine depots. Nat. Immunol. *13*, 67 76.

Steen, A., Larsen, O., Thiele, S., and Rosenkilde, M.M. (2014). Biased and g protein independent signaling of chemokine receptors. Front. Immunol. *5*, 277.

Stephens, B., and Handel, T.M. (2013). Chemokine receptor oligomerization and allostery. Prog. Mol. Biol. Transl. Sci. *115*, 375 420.

Thelen, M., and Stein, J.V. (2008). How chemokines invite leukocytes to dance. Nat. Immunol. *9*, 953 959.

Ulvmar, M.H., Werth, K., Braun, A., Kelay, P., Hub, E., Eller, K., Chan, L., Lucas, B., Novitzky Basso, I., Nakamura, K., et al. (2014). The atypical chemokine receptor CCRL1 shapes functional CCL21 gradients in lymph nodes. Nat. Immunol. *15*, 623 630.

Weber, M., Hauschild, R., Schwarz, J., Moussion, C., de Vries, I., Legler, D.F., Luther, S.A., Bollenbach, T., and Sixt, M. (2013). Interstitial dendritic cell guidance by haptotactic chemokine gradients. Science *339*, 328 332.

Zidar, D.A., Violin, J.D., Whalen, E.J., and Lefkowitz, R.J. (2009). Selective engagement of G protein coupled receptor kinases (GRKs) encodes distinct functions of biased ligands. Proc. Natl. Acad. Sci. USA *106*, 9649 9654.